

# Modeling and Simulation of a Microstrip-SQUID Amplifier

G.P. Berman<sup>a</sup>, O.O. Chumak<sup>b</sup>, D.I. Kamenev<sup>a</sup>, D. Kinion<sup>c</sup>, and V.I. Tsifrinovich<sup>d</sup>

<sup>a</sup>*Theoretical Division, Los Alamos National Laboratory, Los Alamos, NM 87545, USA*

<sup>b</sup>*Institute of Physics of the National Academy of Sciences,  
Pr. Nauki 46, Kiev-28, MSP 03028, Ukraine*

<sup>c</sup>*Lawrence Livermore National Laboratory, Livermore, CA 94551, USA and*

<sup>d</sup>*Department of Applied Physics, Polytechnic Institute of NYU,  
6 MetroTech Center, Brooklyn, NY 11201, USA*

Using a simple lumped-circuit model, we numerically study the dependence of the voltage gain and noise on the amplifier's parameters. Linear, quasi-linear, and nonlinear regimes are studied. We have shown that the voltage gain of the amplifier cannot exceed a characteristic critical value, which decreases with the increase of the input power. We have also shown that the spectrum of the voltage gain depends significantly on the level of the Johnson noise generated by the SQUID resistors.

## I. INTRODUCTION

A microstrip-SQUID (superconducting quantum interference device) amplifier (MSA) has been designed as a low noise radiofrequency amplifier, which is able to operate above 100 MHz [1]. The MSA has been studied theoretically in many publications [1–9]. However, a consistent theoretical model of MSA has not yet been developed. The circuit diagram of lumped model of MSA is presented in Fig. 1. This MSA consists of a linear input circuit coupled to the direct current (dc) SQUID via the mutual inductance,  $M$ . Note that the isolated dc SQUID is a nonlinear circuit, while the isolated microstrip is a linear circuit. The total system consisting of the SQUID and the input circuit is a nonlinear one. Consequently, it remains no trivial task to predict the performance of the MSA during the design process. Therefore analytical investigation and extensive numerical modeling, simulation, and optimization of the MSA are required before creating the device. Generally, the solutions for the MSA model must be obtained by solving analytically or numerically the system of nonlinear ordinary differential equations written for the SQUID coupled to the input circuit. The dynamics of a bare SQUID was investigated numerically in [10–12].

The objective of our paper is to study numerically the dynamics of exact nonlinear equations describing the MSA, and to compute the voltage gain,  $G(f) = |V(f)/V_i|$ , of the MSA, where  $V(f)$  is a Fourier harmonic of the output voltage on the SQUID, and  $V_i$  is the ampli-

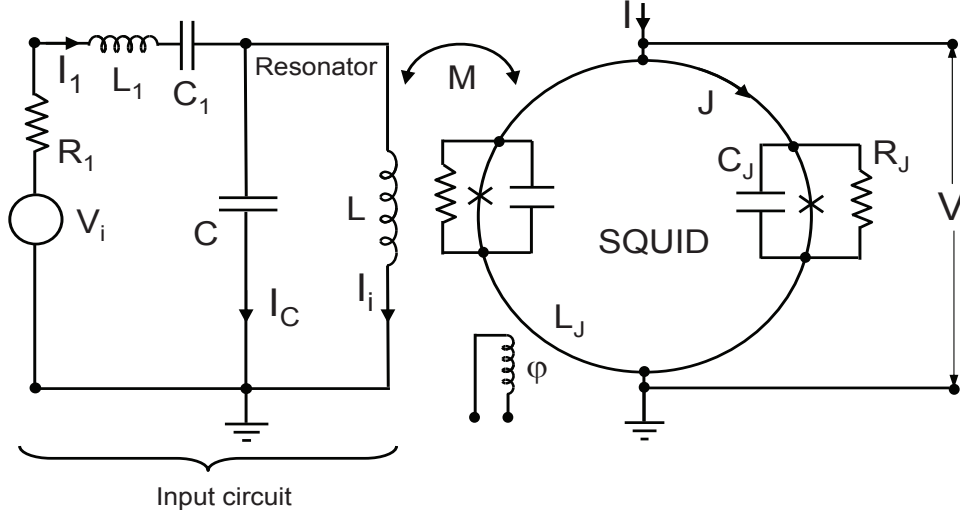


FIG. 1: The equivalent scheme of the microstrip-SQUID amplifier.  $V_i$  is the amplitude of the input voltage and  $R_1$  is the resistance of the voltage source.  $L_1$  describes the stray inductance, and (if necessary) the pick-up coil inductance,  $C_1$  is the coupling capacitance,  $L$  is the inductance of the input coil for the SQUID,  $I$  and  $\varphi$  are, respectively, the bias current and the flux for the SQUID,  $M$  is the mutual inductance between the input coil,  $L$ , and the SQUID loop.  $L_J$  is the inductance of the SQUID loop,  $I_1$ ,  $I_C$ , and  $I_i$  are the currents in the input part of the circuit, and  $J$  is the current circulating around the SQUID loop,  $C_J$  and  $R_J$  are, respectively, the capacitance and resistance of each Josephson junction.

tude of the input voltage on the microstrip at the same frequency,  $f$ . We analyze numerically both linear and nonlinear regimes of amplification. A linear regime means that the following linear dependence exists:  $|V(f)| = G(f)|V_i|$ , where the gain  $G(f)$  is independent of the  $V_i$ . We also simulate the output spectral density of voltage Johnson noise, originated in shunting resistors of the SQUID and the resistor,  $R_1$ , in the input circuit, and calculate the noise temperature.

## II. INPUT CIRCUIT

Consider the isolated linear input circuit ( $M = 0$ ). The forward impedance of the input circuit is

$$Z_i = \frac{V_i}{I_i} = \left( 2\pi i f L_1 + \frac{1}{2\pi i f C_1} + R_1 \right) \left( 1 - (2\pi f)^2 L C \right) + 2\pi i f L. \quad (1)$$

In Fig. 2 we plot the amplitude of the current,  $I_i$ , in the input coil with inductance  $L$ , when  $M = 0$ . One can see from Fig. 2 that as  $C_1$  decreases, the maximum shifts to higher

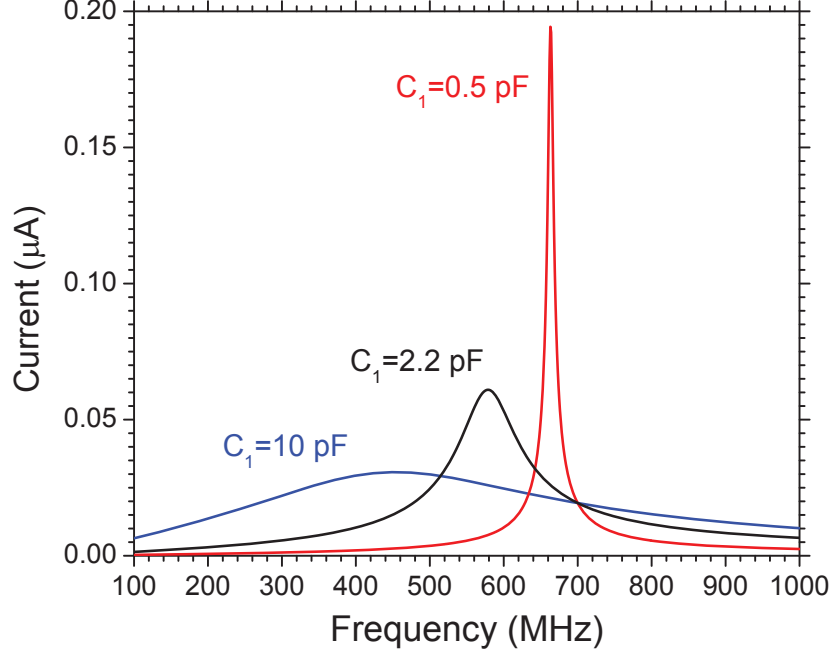


FIG. 2: Current,  $I_i$ , in the input coil for an isolated input circuit ( $M = 0$ ), and for three values of the coupling capacitance,  $C_1$ .  $R_1 = 50 \text{ Ohm}$ ,  $V_i = 1 \text{ } \mu\text{V}$ ,  $L_1 = 1 \text{ nH}$ ,  $C = 4.4 \text{ pF}$ .  $f_0 = 1/(2\pi\sqrt{LC}) = 700 \text{ MHz}$  is the resonant frequency of the input resonator.

frequencies, and the width of the peak decreases. One can use this latter property to create a narrow-bandwidth amplifier. The frequency corresponding to the maximum is always less than the resonant frequency,  $f_0$ , of the input resonator.

### III. EQUATIONS OF MOTION

The differential equations of motion for the SQUID are: [4]

$$\begin{aligned}\varphi_0 C_J \ddot{\delta}_1 + \frac{\varphi_0}{R_J} \dot{\delta}_1 &= \frac{I}{2} - J - I_0 \sin \delta_1 + I_{n1}, \\ \varphi_0 C_J \ddot{\delta}_2 + \frac{\varphi_0}{R_J} \dot{\delta}_2 &= \frac{I}{2} + J - I_0 \sin \delta_2 + I_{n2}, \\ \varphi_0 (\delta_1 - \delta_2) &= \varphi + L_J J + M I_i.\end{aligned}\tag{2}$$

Here the dot above  $\delta_1$  and  $\delta_2$  indicates time differentiation;  $\varphi_0 = \hbar/(2e)$  is the reduced flux quantum;  $\hbar$  is Planck's constant;  $e$  is the electron charge;  $\delta_1$  and  $\delta_2$  are the phase differences in the Josephson junctions in the SQUID;  $I_0$  is the Josephson junction critical current;  $I_{n1}$  and  $I_{n2}$  describe the noise current (Johnson noise) originating in the shunt resistors,  $R_J$ . The

output voltage,  $V$ , can be expressed in terms of the Josephson junction phase differences

$$V = \frac{\varphi_0}{2} (\dot{\delta}_1 + \dot{\delta}_2).$$

In order to determine  $I_i$  in the third equation in (2), we have to add the differential equations for the input circuit. The total system of eight first-order differential equations can be written in the following form:

$$\begin{aligned} \dot{x}_1 &= p_1, \\ \dot{p}_1 &= \frac{1}{C_J} \left( -\frac{1}{R_J} p_1 + I - 2 \sin \frac{x_1}{2\varphi_0} \cos \frac{x_2}{2\varphi_0} + I_{n1} + I_{n2} \right), \\ \dot{x}_2 &= p_2, \\ \dot{p}_2 &= \frac{1}{C_J} \left[ -\frac{1}{R_J} p_2 - \frac{1}{L_J} (x_2 - \varphi - M I_i) - 2 \sin \frac{x_2}{2\varphi_0} \cos \frac{x_1}{2\varphi_0} + I_{n1} - I_{n2} \right], \\ \dot{Q}_1 &= I_1, \\ \dot{I}_1 &= \frac{1}{L_1} \left[ V_i \cos(2\pi f t) + V_n - \frac{Q_1}{C_1} - I_1 R_1 - \frac{Q_C}{C} \right], \\ \dot{Q}_C &= I_1 - I_i, \\ \dot{I}_i &= \frac{1}{L\alpha} \left( \frac{Q_C}{C} - \frac{M}{L_J} p_2 \right). \end{aligned} \quad (3)$$

Here

$$x_1 = \varphi_0(\delta_1 + \delta_2); \quad x_2 = \varphi_0(\delta_1 - \delta_2); \quad \alpha = 1 - \frac{M^2}{LL_J};$$

$Q_1$  is the charge on the capacitor  $C_1$ ;  $Q_C$  is the charge on the capacitor  $C$ ;  $f$  is the frequency of the external voltage; and  $V_n = I_n R_1$  is the noise voltage on the the resistor  $R_1$ ;  $I_n$  is the noise current through  $R_1$ .

The input circuit is coupled to the SQUID through the term,  $M I_i / (C_J L_J)$ , in the fourth equation in (3), and the SQUID is coupled to the input circuit by the effective coupling constant,  $\gamma = M / (L L_J \alpha)$ , in the last equation in (3). Since the effective coupling constant,  $\gamma$ , is proportional to  $1/\alpha$ , the effective coupling can be increased by decreasing  $\alpha$ .

#### IV. VOLTAGE GAIN

First we choose the optimal working point of our amplifier which is defined by the value of  $\varphi$ , provided the other parameters are given. In Fig. 3 the time average,  $V_0$ , of the output voltage and its derivative (transfer function) are plotted as a function of  $\varphi$ . The maximum of the transfer function occurs in the vicinity of  $\varphi/\varphi_0 = 0.3$  which we choose as our working point.

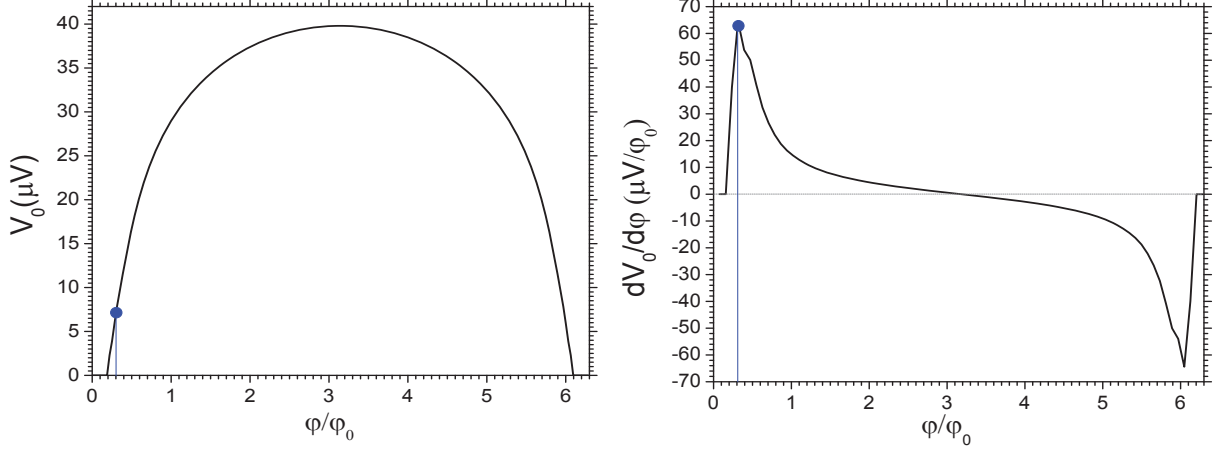


FIG. 3: Average over time of the output voltage,  $V_0$ , (left) and its derivative (transfer function) (right). The working point for  $\varphi/\varphi_0 = 0.3$  is marked by a filled blue circle.  $C_J = 0.2$  pF,  $L_J = 0.45$  nH,  $R_J = 20$  Ohm,  $I = 1.99I_0$ ,  $I_0 = 2$   $\mu$ A,  $\alpha = 0.001$ ,  $C_1 = 0.5$  pF,  $V_i = 0$ ,  $I_{n1} = I_{n2} = 0$ . The other parameters are the same as in Fig. 2.

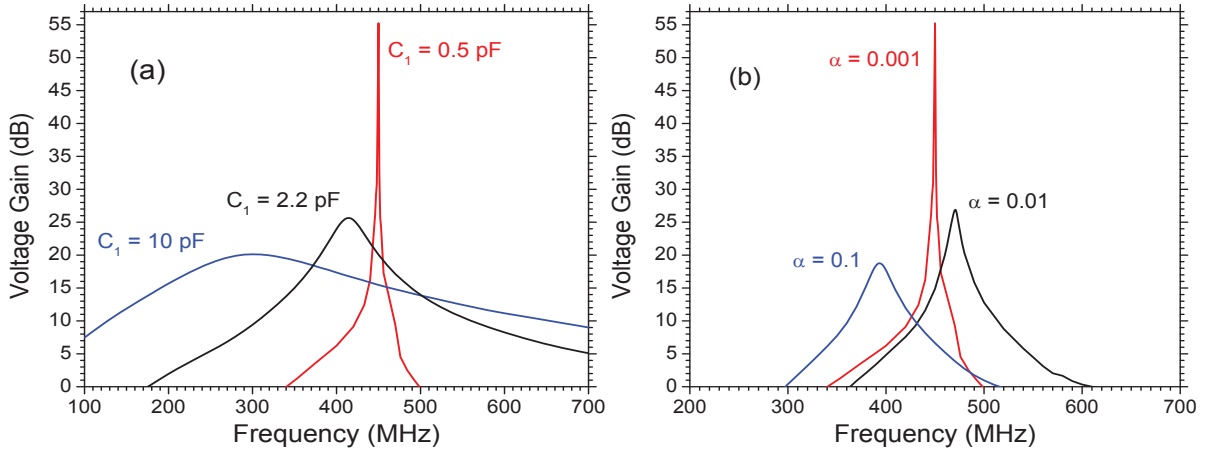


FIG. 4: (a) Voltage gain of the amplifier for three values of the coupling capacitance,  $C_1$ , and for  $\alpha = 0.001$ . (b) Voltage gain for three values of  $\alpha$ , and for  $C_1 = 0.5$  pF.  $V_i = 0.001$   $\mu$ V in both (a) and (b). The other parameters are the same as in Figs. 2 and 3.

In Fig. 4(a) we plot the voltage gain for three values of the coupling capacitance,  $C_1$ . By comparison of Fig. 4(a) with Fig. 2, one can conclude that the amplifier gain is mostly defined by the parameters of the input circuit. The gain of 55 dB for  $C_1 = 0.5$  pF is the combined result of amplification by the input circuit and by the SQUID due to the strong interaction between them when  $\alpha$  is small and positive. Note that the dimensionless parameter,  $\alpha$ , contains both the parameters of the SQUID ( $L_J$ ) and the input circuit ( $L$ ), as well as the coupling inductance,  $M$ . In Fig. 4(b) we plot the gain for three values of

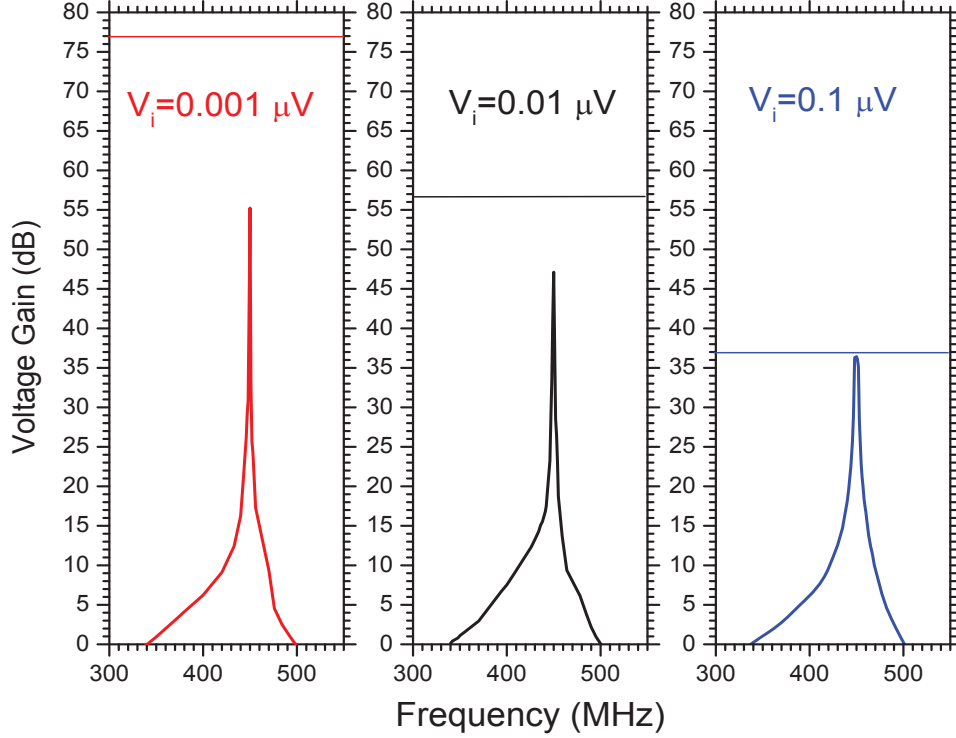


FIG. 5: Voltage gain for three values of input voltage amplitude  $V_i$ .  $\alpha = 0.001$ ,  $C_1 = 0.5$  pF, the other parameters are the same as in Figs. 2 and 3.

$\alpha$ :  $\alpha = 0.001, 0.01$ , and  $0.1$ . The gain decreases from 55 dB to 27 dB as  $\alpha$  increases from 0.001 to 0.01. The value of coupling inductance,  $M$ , changes, respectively, from 2.2982 nH to 2.2878 nH, that is, by only 0.44 percent. Therefore, the possibility of obtaining the large gain is limited to a very small region of the parameters. For this purpose it is desirable to have a tunable coupling inductance,  $M$ , or a tunable input circuit inductance,  $L$ , or a tunable SQUID inductance,  $L_J$ .

Consider the situation in which  $\alpha$  is negative, that is  $M^2 > LL_J$ . In order to understand the dynamics in this regime, we differentiate the last equation in (3) and use the 4th and 7th equations for  $\dot{Q}_C$  and  $\dot{p}_2$ . We obtain an equation for the oscillations of the input current,  $I_i$ , with an external force and with the eigenfrequency,  $\omega_0$ , where

$$\omega_0^2 = \frac{1}{\alpha} \left( \frac{1}{LC} + \frac{M^2}{L_J^2 LC_J} \right).$$

Negative  $\alpha$  corresponds to negative real part of the input impedance [13, 14]. This regime can drive the resonator into instability [15].

## V. NONLINEARITY

When the input voltage amplitude or gain becomes sufficiently large, the nonlinear effects in the SQUID become important. In the nonlinear regime, the nonlinear effects decrease the output voltage of the SQUID, thus decreasing the gain of the amplifier in comparison with the linear regime. It is reasonable to assume that the MSA is in the nonlinear regime when the output voltage becomes comparable with the SQUID's own average output voltage,  $V_0$ . It is convenient to define the maximum gain

$$G_{max} = \left| \frac{V_0}{V_i} \right|. \quad (4)$$

When the amplitude,  $|V(f)|$ , of the amplified output Fourier harmonic approaches  $|V_0|$ , the gain should decrease due to nonlinear effects in the SQUID. If, for example, the amplitude of the input signal is  $V_i = 1 \mu\text{V}$  and  $V_0 = 7 \mu\text{V}$  (see left side in Fig. 3 for  $\varphi/\varphi_0 = 0.3$ ), according to Eq. (4) the gain is limited by the value  $G_{max} = 7$ . In order to obtain a gain of  $G = 55 \text{ dB}$  in Figs. 4(a) and (b), we set the amplitude of the input signal to be  $V_i = 0.001 \mu\text{V}$ . For this input signal expressed in decibels [ $G_{max}(\text{dB}) \rightarrow 20 \log_{10} G_{max}$ ], we have  $G_{max} = 76.9 \text{ dB}$ , so that  $G(f) < G_{max}$ . For  $V_i = 0.01 \mu\text{V}$ , we have  $G_{max} = 56.9 \text{ dB}$ , and for  $V_i = 0.1 \mu\text{V}$  one obtains  $G_{max} = 36.9 \text{ dB}$ . In Fig. 5 we plot the gain,  $G(f)$ , for three values of  $V_i$ . One can see from the figure that  $G(f)$  is less than  $G_{max}$  for all frequencies,  $f$ . (The values of  $G_{max}$  for each  $V_i$  are indicated in the figures by the horizontal lines.) In Fig. 6(a) we plot  $G$  as a function of  $V_i$ . As follows from the figure, the condition  $G < G_{max}$  is also satisfied for all input voltage amplitudes,  $V_i$ . As the amplitude,  $V_i$ , of the input signal increases, both  $G_{max}$  in Eq. (4) and the gain,  $G$ , decrease. This nonlinear effect cannot be obtained from a linearized theory, like that based on an effective impedance of the amplifier [16]. In Fig. 6(b) the amplifier is in the linear regime for  $C_1 = 2.2 \text{ pF}$  and  $C_1 = 10 \text{ pF}$  because the gain is sufficiently small,  $G \ll G_{max}$ .

## VI. NOISE

We assume that the Johnson noise voltages across the resistors dominate all other sources of noise in the amplifier. White Gaussian noise in each of three resistors was modeled by a train of rectangular pulses following each other without interruption. The current amplitude,  $I_n$ , of each pulse is random with zero average and the following variance:

$$\langle I_n^2 \rangle = 2 \frac{k_B T}{R \Delta t}.$$

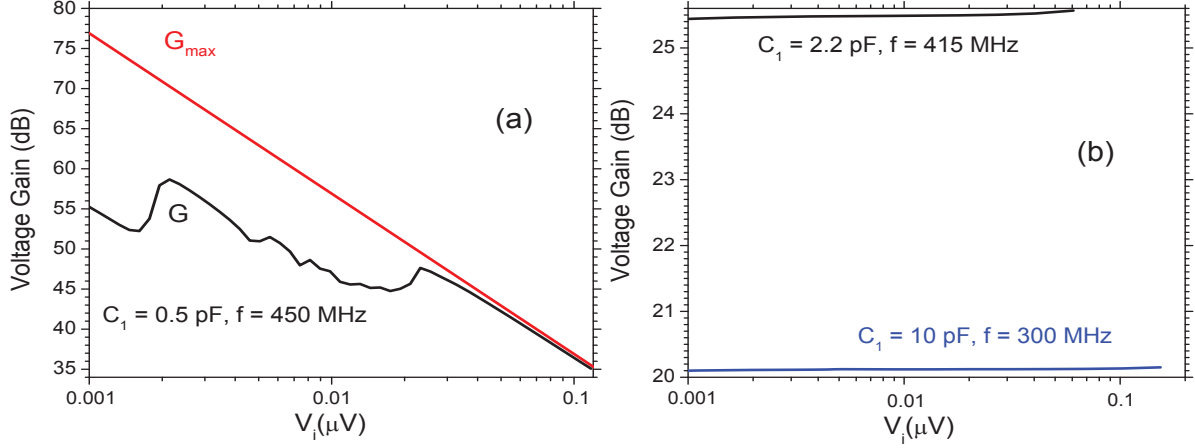


FIG. 6: (a) Voltage gain,  $G$ , and maximum gain,  $G_{\text{max}}$ , as a function of the input voltage amplitude,  $V_i$ . In maximum  $G = 58.7 \text{ dB}$  (black curve). (b) Voltage gain,  $G$ , in linear regime as a function of the input voltage amplitude,  $V_i$ .  $\alpha = 0.001$  and the other parameters are the same as in Figs. 2 and 3.

Here the brackets indicate an average over different realizations;  $k_B$  is the Boltzmann constant;  $T$  is the temperature of the MSA;  $\Delta t$  is the duration of each pulse, which is constant in our simulations;  $R$  is the corresponding resistance:  $R = R_J$  for the shunting resistors in the SQUID and  $R = R_1$  for the resistor  $R_1$  in the input circuit. In Fig. 7 we plot the output voltage spectral density,  $S_V(f)/S_V^0$  (where  $S_V^0 = \varphi_0 I_0 R_J$ ), when no input voltage is applied to the input circuit,  $V_i = 0$ .  $S_V$  is defined as:

$$S_V = \lim_{t_i \rightarrow \infty} \frac{2}{t_i} \langle |V(f)|^2 \rangle, \quad V(f) = \int_0^{t_i} V(t) e^{2\pi i f t} dt,$$

where  $t_i$  is the time of integration of the output signal and the angular brackets,  $\langle \rangle$ , indicate an average over different realizations.

One can use the voltage spectral density,  $S_V(f)$ , to calculate the noise temperature of the amplifier,  $T_1$ , using the following equation:

$$4k_B(T_1 + T)R_1 |G(f)|^2 = S_V(f).$$

In Fig. 8 we plot  $T_1/T_q$ , as a function of frequency,  $f$ , for two different scales, where  $T_q = hf/k_B$  is the quantum temperature. We use the noise spectral density,  $S_V(f)$ , from Fig. 7 and the gain from Fig. 4(a). At the minimum, for  $C_1 = 0.5 \text{ pF}$  (red line) the noise temperature is negative.

We now show that this negative noise temperature is related to the method of its calculation. The reason for the negative noise temperatures is in the different methods of calculation of the noise spectral density and the gain of the amplifier. There are three resistors that act



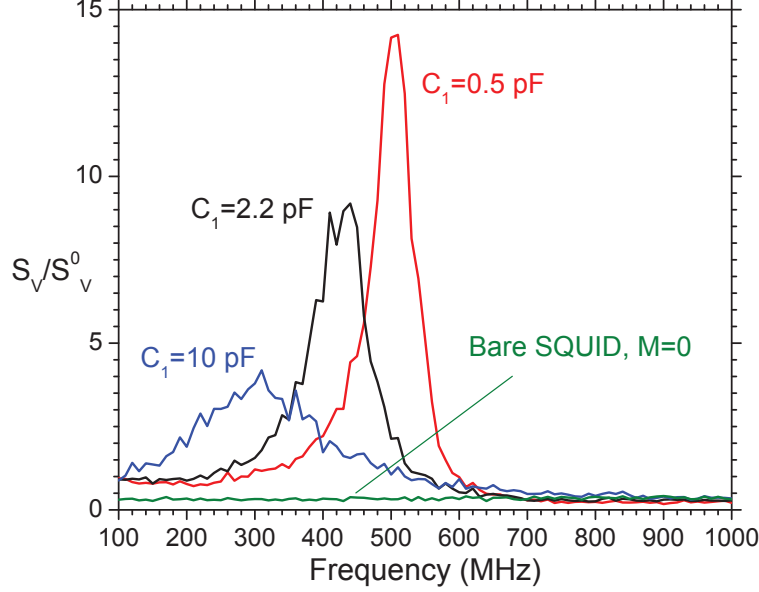


FIG. 7: Output voltage spectral density  $S_V/S_V^0$ , where  $S_V^0 = \varphi_0 I_0 R_J$ , as a function of frequency,  $f$ , for three values of  $C_1$ ,  $\alpha = 0.001$ . For comparison, we also include the plot of  $S_V/S_V^0$  for bare SQUID (when  $M = 0$ ) with white noise spectral density (because the frequency,  $f$ , is much smaller than the Josephson frequency). The time of integration is  $t_i = 10^4 t_0$ , where  $t_0 = \varphi_0 / (I_0 R_J) = 8.23 \times 10^{-12}$  s; the number of realizations is  $N = 100$ ;  $T = 100$  mK;  $\Delta t = 0.1 t_0$ ;  $V_i = 0$ ; the other parameters are the same as in Figs. 2 and 3.

as sources of noise: two resistors,  $R_J$ , in the SQUID and the resistor,  $R_1$ , in the input circuit. All three resistances contribute to the noise spectral density,  $S_V$ . The noise current in the SQUID, besides contributing to noise spectral density, changes the SQUID's parameters, including the frequency at which the gain is maximum. At one moment the SQUID is tuned to one frequency and at the next moment it is tuned to another frequency. The noise voltage generated in the resistor,  $R_1$ , is amplified by the detuned SQUID. On the other hand, the signal is amplified by the SQUID tuned to a definite frequency because there are no noise currents in the resistors,  $R_J$ , of the SQUID. Consequently the amplification of the signal is greater than the amplification of the noise. Besides, the noisy SQUID shifts the frequency at which the amplification is maximum. In Fig. 4(a) the maximum is at  $f_{max} = 450$  MHz, while in Fig. 7 the maximum is at 510 MHz.

By this argument, we calculated the gain (Fig. 9) and the noise temperature (Fig. 10) with noise on the resistors,  $R_J$ , and with the input signal,  $V_i \neq 0$ . The calculated gain in Fig. 9 is qualitatively similar to that measured experimentally in Ref. [17]. If the time of integration is sufficiently long, the contribution of the noise to the gain is minimized, so only the contribution from the amplified signal remains (see Fig. 11). In this situation

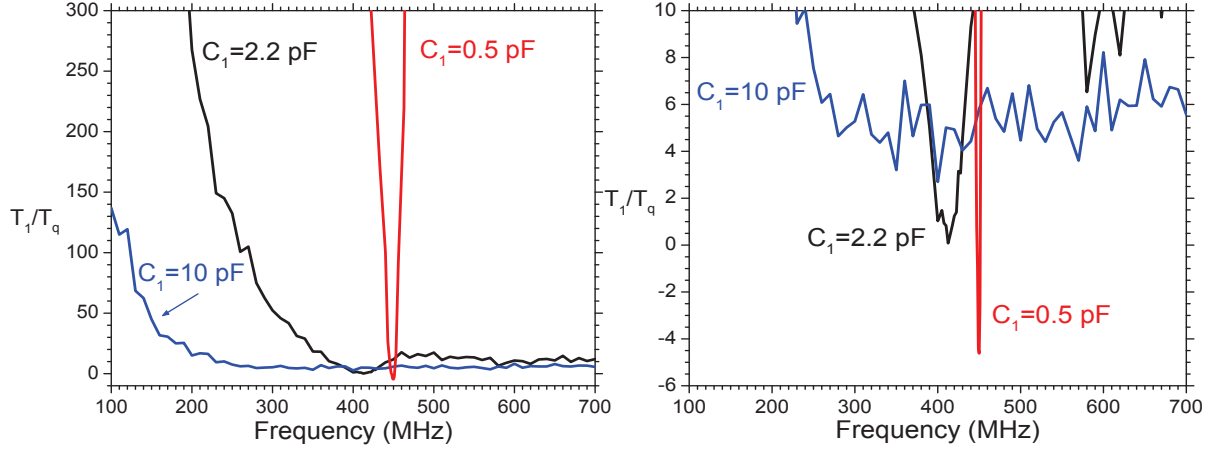


FIG. 8: Noise temperature  $T_1/T_q$  for three values of  $C_1$  in two different scales. The other parameters are the same as in Fig. 4(a) and Fig. 7.

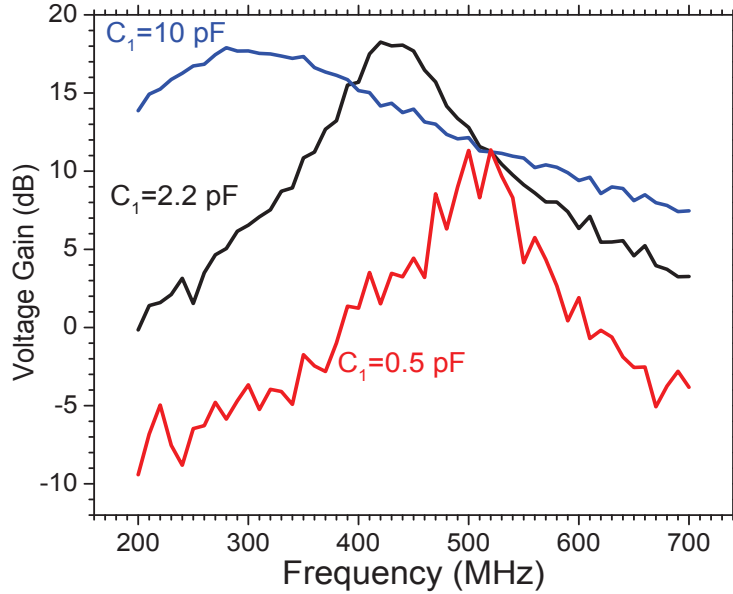


FIG. 9: Gain of the MSA with the noisy SQUID.  $t_i = 10^6 t_0$ ;  $V_i = 0.1 \mu\text{V}$ ;  $N = 10$ ;  $\alpha = 0.001$ ;  $T = 100 \text{ mK}$ . The other parameters are the same as in Fig. 4(a).

both the voltage spectral density and the gain are calculated for the same system with the noisy (detuned) SQUID. Note that a significant asymmetry of the spectrum for  $C_1 = 2.2 \text{ pF}$  and  $10 \text{ pF}$  in Figs. 8 and 10 appears because we plot the ratio  $T_1/T_q$ , where the quantum temperature  $T_q$  is proportional to the frequency  $f$ .

We demonstrated two methods of calculating gain and noise temperature of the MSA. The noise on the shunting resistors of the SQUID reduces gain of the amplifier if one compares Figs. 4(a) (no noise) with Fig. 9 (with noise). The reduction is large for small capacitance,  $C_1 = 0.5 \text{ pF}$ , while the gain for  $C_1 = 10 \text{ pF}$  is mostly not affected by the noise in the

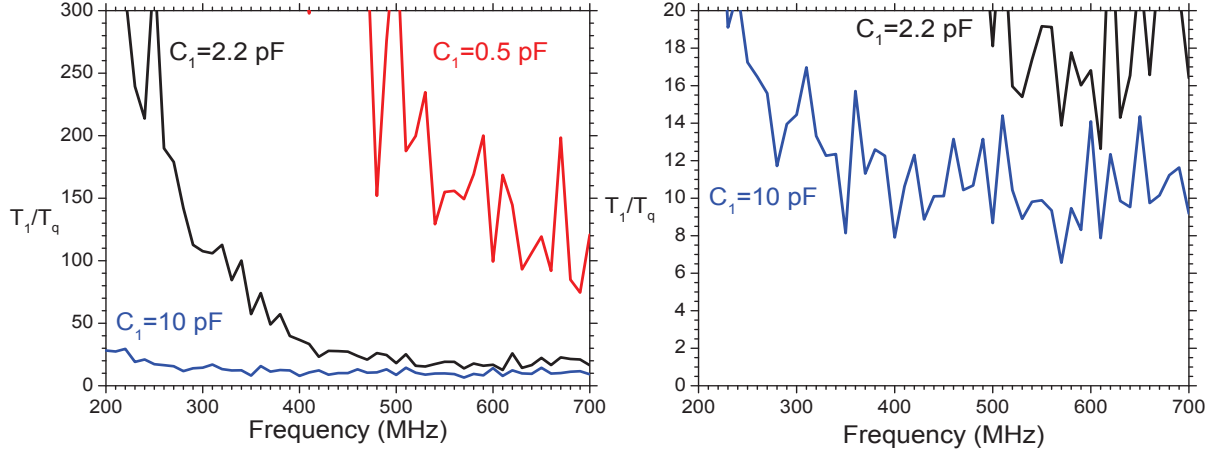


FIG. 10: Noise temperature of the MSA with the noisy SQUID in two different scales. The parameters are the same as in Fig. 9.

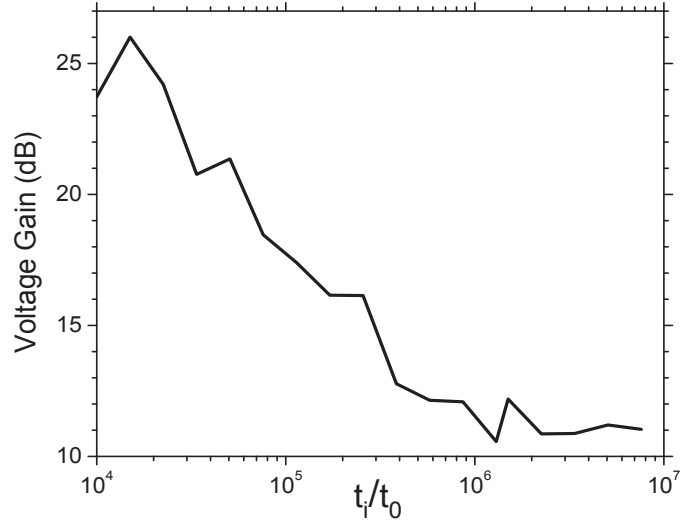


FIG. 11: Gain of the MSA with the noisy SQUID calculated using different integration time,  $t_i$ . The contribution to the gain from the noise on the SQUID decreases as the integration time,  $t_i$ , increases. For  $t_i/t_0 \geq 10^6$  the gain is mostly independent of  $t_i$  which indicates that only contribution from the signal remains.  $C_1 = 0.5$  pF; the other parameters are the same as in Fig. 9.

SQUID. The gain calculated in the previous sections of this paper is actually the gain at zero temperature.

In summary, we have simulated the dynamics of the microstrip-SQUID amplifier in both the linear and nonlinear regimes and studied the dependence of the voltage gain and noise on the parameters of the amplifier. We have shown that the voltage gain cannot exceed the critical value  $G_{max}$  given by the formula (4). This value is inversely proportional to the input voltage. It is shown that the gain decreases as the device temperature increases. Finally, we

have shown that the spectrum of the voltage gain depends significantly on the level of the Johnson noise in the SQUID resistors. This effect must be taken into account for correct calculation of the amplifier noise temperature. The next important step should be the optimization of the gain and noise temperature with respect to the amplifier's parameters.

### Acknowledgements

This work was carried out under the auspices of the National Nuclear Security Administration of the U.S. Department of Energy at Los Alamos National Laboratory under Contract No. DE-AC52-06NA25396 and by Lawrence Livermore National Laboratory under Contract DE-AC52-07NA27344. This research was funded by the Office of the Director of National Intelligence (ODNI), Intelligence Advanced Research Projects Activity (IARPA). All statements of fact, opinion or conclusions contained herein are those of the authors and should not be construed as representing the official views or policies of IARPA, the ODNI, or the U.S. Government.

- 
- [1] J. Clarke, M. Hatridge, and M. Mossle, *Annu. Rev. Biomed. Eng.* **9**, 389 (2007).
  - [2] M. Mück and R. McDermott, *Supercond. Sci. Technol.*, **23**, 093001 (2010).
  - [3] M. Mück and J. Clarke, *J. Appl. Phys.*, **88**, 6910 (2000).
  - [4] J. Clarke, T. L. Robertson, B. L. T. Plourde, A. Gacsia-Martines, P. A. Reichardt, D. J. Van Harlingen, B. Chesca, R. Kleiner, Y. Makhlin, G. Shon, A. Shnirman, and F. K. Wilhelm, *Phys. Scripta* **102**, 173 (2002).
  - [5] B. L. T. Plourde, T. L. Robertson, P. A. Reichardt, T. Hime, S. Linzen, C.-E. Wu, and J. Clarke, *Phys. Rev. B* **72**, 060506 (2005).
  - [6] M. Hamalainen, R. Hari, R. J. Ilmoniemi, J. Knuutila, and O. V. Lounasmaa, *Rev. Mod. Phys.* **65**, No. 2, 413 (1993).
  - [7] R. Bradley, J. Clarke, D. Kinion, S. Matsuki, M. Muck, and P. Sikivie, *Rev. Mod. Phys.* **75**, 777 (2003).
  - [8] S. Michotte, *Appl. Phys. Lett.* **94**, 122512 (2009).
  - [9] M. Mück, J. B. Kycia, and J. Clarke, *Appl. Phys. Lett.* **78**, 967 (2001).
  - [10] C. D. Tesche, and J. Clarke, *IEEE Transactions on Magnetics*, v. MAG-13, No. 1, 859 (1977).
  - [11] C. D. Tesche, and J. Clarke, *J. Low Temp. Phys.*, **29**, 301 (1977).
  - [12] C. D. Tesche *J. Low Temp. Phys.*, **44**, 119 (1981).

- [13] C. Hilbert and J. Clarke, J. Low Temp. Phys., **61**, 237 (1985).
- [14] P. Falferi, R. Mezzena, S. Vitale, M. Cerdonio, Appl. Phys. Lett. **71**, 965 (1997).
- [15] A. Vinante, M. Bonaldi, P. Falferi, M. Cerdonio, R. Mezzena, G. A. Prodi, and S. Vitale, Physica C, **368**, 176 (2002).
- [16] J. M. Martinis and J. Clarke, J. Low Temp. Phys., **61**, 227 (1985).
- [17] D. Kinion and J. Clarke, Appl. Phys. Lett., **92**, 172503 (2008).